Dual Channel Colocalization for Cell Cycle Analysis Using 3D Confocal Microscopy

Stefan Jaeger, Kannappan Palaniappan
Department of Computer Science
University of Missouri
Columbia, USA
Email: {jaegers, pal}@missouri.edu

Corella S. Casas-Delucchi, M. Cristina Cardoso
Department of Biology
Technische Universität Darmstadt
Darmstadt, Germany
Email: {casas, cardoso}@bio.tu-darmstadt.de

***Abstract*—We present a cell cycle analysis that aims towards improving our previous work by adding another channel and using one more dimension. The data we use is a set of 3D images of mouse cells captured with a spinning disk confocal microscope. All images are available in two channels showing the chromocenters and the fluorescently marked protein PCNA, respectively. In the present paper, we will describe our recent colocalization study in which we use Hessian-based blob detectors in combination with radial features to measure the degree of overlap between both channels. We show that colocalization performed in such a way provides additional discriminative power and allows us to distinguish between phases that we were not able to distinguish with a single 2D channel.**

***Keywords*-confocal microscopy; cell cycle analysis; colocalization;**

I. Introduction

The knowledge of cell cycle progress is important in understanding various diseases, e.g. cancer [1], [2]. Getting a better understanding of changes in the cell cycle before and after drug treatment is important for discovering new effective drugs. Our main motivation and long-term interest lies in the effects of different epigenetic modifications on the replication of specific regions of the genome [3]. To this end, we manipulated one of these epigenetic modifications using a drug and looked at the effects on replication timing by live cell microscopy labeling both the regions of interest as well as replication sites. Our immediate objective for these data is twofold: First, we want to learn how the treatment changes the (relative) duration of each cell cycle stage, including the subphases of S-phase (SE/SM/SL), which are hard to distinguish [4]. Compared with the literature on general cell cycle analysis, trying to distinguish also the sub-phases of S-phase with colocalization is a less explored area. Second, we want to find out if the treatment increases the colocalization of both signals at particular cell cycle stages.

The biological details and replication timing, however, are out of the scope of this paper. In the following, we will concentrate exclusively on the description of individual cell cycle phases and colocalization, which is a necessary step to reach our long-term goal. An automated approach to this is preferable as test series in practice typically produce vast amounts of data that are prohibitive to evaluate manually [5]. The paper is an extension of our earlier work [6] in that it uses both 3D data, instead of merely 2D, and an additional data channel.

We structured the paper as follows: Section 2 describes the biological background and the data used in our experiments. Section 3 shows how we segment individual cells, implement Hessian blob detection, and compute radial features. Finally, Section 4 presents our results, followed by a summary concluding the paper.

II. Biological Motivation

A replicating cell typically undergoes the following cell cycle: After the cell divides (mitosis/ M-phase), it enters the G1-phase. Following the G1-phase, after completing a series of "tasks" such as cell growth, the cell starts preparing for the next division by duplicating its DNA. This is what we call S-phase and when we actually start seeing structures or replication foci. S-phase progresses from early S-phase (SE) via mid S-phase (SM) to late S-phase (SL). When the cell has duplicated its entire DNA, it enters the G2-phase, where it checks for different criteria so it can divide again.

We use two channels for our experiments, namely chromocenters and replication structures. The chromocenters are structures built by specific regions of DNA, the major satellites. The left-hand column of Figure 1 shows the chromocenters of a cell slice in SE, SM, and SL-phase, respectively. The visual appearance of the chromocenters in the first channel is relatively stable throughout the different stages of the cell cycle, except for the G2-phase. At the end of G2, chromosomes start condensing for mitosis. When this happens (prometaphase), chromosomes can be seen as individual entities. This automatically causes that chromocenters, which are usually clusters of heterochromatin of several chromosomes, change their shape and appear as elongated objects.

The replication structures in the second channel are foci of fluorescently marked PCNA/ RFP-PCNA (proliferating cell nuclear antigen), a protein involved in DNA replication and repair. It is mainly the second channel (i.e. replication foci/PCNA) that can give us information on a cell's cycle stage. While PCNA is homogeneous during G1-phase and G2-phase, and much diluted during M-phase, it produces a

1051-4651/10 $26.00 © 2010 IEEE
DOI 10.1109/ICPR.2010.632

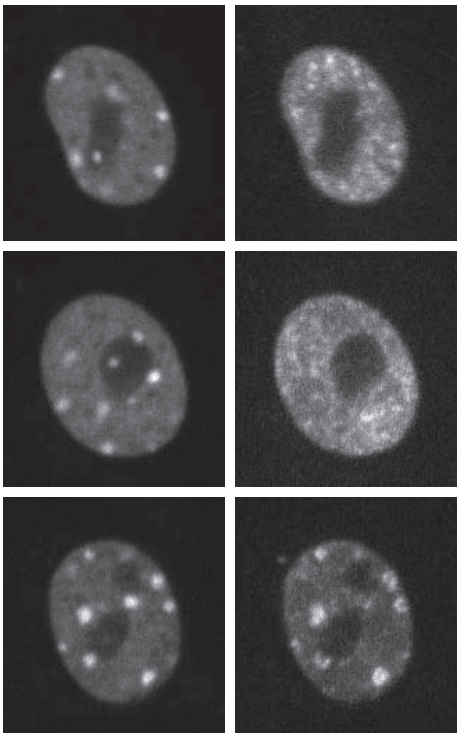

Figure 1. Chromocenters (left column) and PCNA (right column) in SE (top row), SM (middle row), and SL-phase (bottom row).

complex distribution of foci pattern in different stages of S-phase [7], [8]. The right-hand column of Figure 1 shows the PCNA of a cell slice in SE, SM, and SL-phase, respectively. As soon as we start seeing defined structures, i.e. small foci distributed almost all over the nucleus, we say early S-phase has started. At this point, the nucleolar and nucleolar rim are rather free of replication. Then, as replication structures begin to populate these regions, mid S-phase starts. The beginning of the replication of the chromocenters marks the start of late S-phase, in which we can see pronounced foci (see Figure 1).

The examples show that it is difficult to distinguish between subphases of S-phase with only one channel. In terms of cell cycle phase discrimination, the sub-phases of S are the hardest to discriminate due to the difficulty in clearly seeing the PCNA foci distribution, particularly between SE and SM, as we have shown in our earlier work for 2D data in [6]. In addition, these phases can often be confused with a so-called "very late" S-phase, which starts when the chromocenters have almost finished replicating and there are still a few smaller foci distributed in the nucleus. This is when the last unreplicated DNA pieces start replicating before G2, mostly outside the chromocenters. Another phase pair that is hard to distinguish is G1 and SE. In this paper, we try to improve our discriminative power for SE/SM/SL by using 3D confocal spinning disc data and an additional channel, namely chromocenters, compared to the single PCNA channel used in our earlier work [6]: The chromocenter regions characteristically replicate during late S-phase, so the degree of colocalization with the replication structures in the second channel allows us to check for late S-phase patterns.

III. Colocalization for Cell Cycle Phase Classification

In our approach, colocalization proceeds in three steps: First, we segment the individual cell nuclei from each image stack. Then, we compute blob descriptors for each segmented nucleus. Finally, we compute histograms that, simply speaking, count the number of blobs for different radii around a cell's nucleus center in 3D. This reduces colocalization to a distance computation between histograms [9], [10]. The following subsections describe this approach in more detail.

A. Nuclei Segmentation Using Adaptive Thresholding

Segmentation in live cell imaging has been subject of intensive research in recent years. Many authors use level-set methods to cope with the various challenges that come with bioimages, e.g. [11], [12], [13]. In our work, however, we use a modified k-means clustering approach and adaptive thresholding to extract individual cells. We found that this approach works fairly well on our data, and that the clusters represent the different intensities of cells, halos, and background quite nicely in our case. In particular, we optimize the standard k-means expression

$$\underset{S}{\operatorname{argmin}} \sum_{i=1}^{k} \sum_{x_j \in S_i} \|x_j - \mu_i\|^2 \tag{1}$$

where the x_j represent the different voxel intensities and μ_i stands for the mean of cluster S_i. The clusters of the final cell segmentation are given by

$$S_{seg} = \{S_i \,|\, \bar{S}_i \geq \gamma * max_i(\bar{S}_i)\} \tag{2}$$

with $0 \leq \gamma \leq 1$, where $\bar{S}_i$ denotes the average intensity of all pixels belonging to cluster S_i and $max_i(\bar{S}_i)$ is the maximum of all these averages. The idea is to make k-means more robust against noise by considering intensity averages. For our experiments, we set $\gamma = 0.5$. The right-hand side of Figure 2 shows a typical segmentation of a nucleus.

B. Hessian-based Foci Detection

For detecting subcellular foci or generically blobs, which represent either chromocenters or PCNA in our application, we follow a method by Frangi et al. [14], [15]. They use a multi-scale approach that analyzes the eigenvalues of the Hessian matrix. Their method, however, tries to detect vessels and thus employs a similarity measure that is not suitable for blob detection. We have therefore slightly modified their method for blob detection.

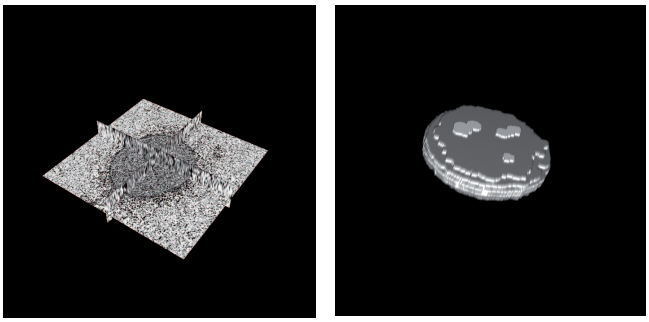

Figure 2. Cross-section (left) and segmentation (right) of a nucleus.

A typical way to describe the local behavior of an image L is to consider its Taylor expansion in the neighborhood of a point x_o (up to the second order):

$$L(x_o + \delta_{x_o}, s) \approx L(x_o, s) + \delta x_o^T \nabla_{o,s} + \delta x_o^T \mathcal{H}_{o,s} \delta x_o \quad (3)$$

where $\nabla_{o,s}$ and $\mathcal{H}_{o,s}$ are the gradient vector and Hessian matrix of the image computed at x_o for scale s. In the framework of Frangi et al., differentiation is defined as a convolution with derivatives of Gaussians [14]:

$$\frac{\partial}{\partial x} L(x, s) = s^\gamma L(x) * \frac{\partial}{\partial x} G(x, s) \quad (4)$$

where the D-dimensional Gaussian is defined by

$$G(x, s) = \frac{1}{\sqrt{(2\pi s^2)^D}} \, e^{-\frac{\|x\|^2}{2s^2}} \quad (5)$$

and the parameter γ weights the response of differential operators at multiple scales. When γ is set to unity, no scale is preferred.

We use the following measure to detect spherical blobs

$$B = \frac{|\lambda_1|}{\sqrt{|\lambda_2 \lambda_3|}} \quad (6)$$

where $\lambda_1, \lambda_2, \lambda_3$ are the eigenvalues of the Hessian, with $|\lambda_1| \leq |\lambda_2| \leq |\lambda_3|$. This ratio attains its maximum for a blob-like structure and is zero whenever $\lambda_1 \approx 0$, or λ_2 and λ_3 tend to vanish [14]. We analyze this "blobbiness" feature at different scales s. The response will be maximum at a scale that approximately matches the size of the detected blob. The final measure is then the integrated filter response at different scales (see [16] for more information about spherical tensors).

C. Radial Features

To quantify the blobbiness in different regions of the image, we compute radial features for the similarity measure defined by Eq. 6 for each voxel of the segmented nucleus. In particular, given the k-means cell segmentation as described above, we compute the i-th radial feature R_i for each voxel in the cell nucleus as follows

$$R_i = \sum_{x,y,z} d_i(B_{xyz}, x, y, z) \quad (7)$$

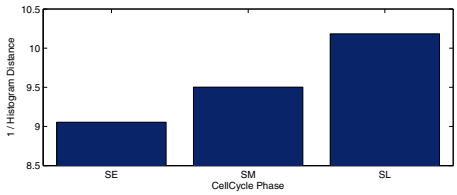

Figure 3. Colocalization between chromocenters and PCNA for SE, SM, and SL phases.

where B_{xyz} denotes the computed blobbiness measure for the voxel at position (x, y, z) in the original image L, and $d_i(B_{x,y,z}, x, y, z)$ checks the distance to the cell boundary based on a distance transform computed on the segmented image. If the distance of L_{xyz} to the cell boundary is i, then $d_i(B_{xyz}, x, y, z)$ returns B_{xyz}; otherwise, it returns zero.

IV. Experimental Results

We use a spinning disk confocal microscope to capture non-fixed live mouse cells (MEF) in various cell cycle stages. Note that the foci structure patterns in mouse cells typically differ from the patterns observed in human cells. With a spinning disk confocal microscope, we can achieve both high resolutions and high-throughput data rates at the same time. We acquired 3D stacks every 30 min for several hours (typically between 10 and 40 hours). The stacks have an XY resolution of 100nm and a z-step of 500nm. Each stack contains slices with 1000x1000 pixels, where the number of slices (z-steps) varies per experiment. From the set of captured stacks, we cropped the regions of interest by hand. We also cropped in z-direction to eliminate slices without any information, thus reducing the data volume and the computational costs. In a later step, we plan to automate this manual segmentation step.

In our experiment, we used six shades of gray for the k-means segmentation; i.e. $k = 6$, and 10 radii for the radial features. The value of k, which we determined empirically, has a significant impact on the segmentation quality. Our database contains about 300 images for both channels. An image stack can consist of up to 50 frames, with the typical size between ten and twenty slices. The size of the slices can vary too, but it is usually either 260×260 or 300×300.

Figure 3 shows the average colocalization between the radial features of the first and second channel for SE/SM/SL, where we use the Euclidean distance to compute the difference between histograms. We can see that the blob distributions are becoming more similar with time progressing from SE to SL. Figure 4 shows the radial blobbiness for a cell in SL-phase. For each radial distance on the x-axis, the y-axis displays the relative number of blobs having that particular distance to the center of the cell's nucleus, where we binned radial distances into ten bins. The solid line in Figure 4 shows the distribution of blobs for chromocenters, while the dashed line shows the distribution for PCNA. We

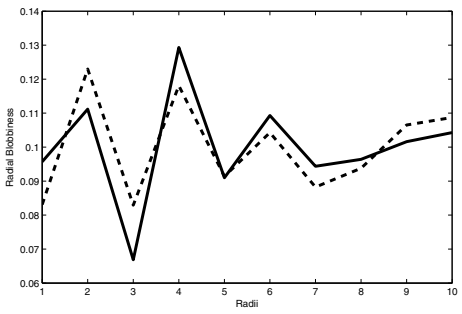

Figure 4. Radial features of chromocenters (solid) and PCNA (dashed) for a cell in SL-phase.

can see a strong correlation; i.e. colocalization, between both channels.

V. Conclusions

We have shown that a Hessian blob detector in combination with radial features can capture the subtle distribution differences of cell cycle phases in multi-channel 3D confocal microscopy. This allows us to discriminate more effectively between different cell cycle phases and describe the ongoing biological processes quantitatively. In particular, we are now able to discriminate between SE/SM/SL phases, which was not possible in our previous 2D approach with only one PCNA channel. In future work, we plan to compute improved 3D classification rates for all cell cycle phases in our data set, including the subphases of S-phase.

Acknowledgment

Part of this work was funded by grants from the Deutsche Forschungsgemeinschaft (DFG) to M.C.C.

References

[1] M. Wang, X. Zhou, F. Li, J. Huckins, R. King, and S. Wong, "Novel cell segmentation and online SVM for cell cycle phase identification in automated microscopy," *Bioinformatics*, vol. 24, no. 1, pp. 94–101, 2008.

[2] T. Buck, A. Rao, L. Coelho, M. Fuhrman, J. Jarvik, P. Berget, and R. Murphy, "Cell cycle dependence of protein subcellular location inferred from static, asynchronous images," in *Int. Conf. of the IEEE Engineering in Medicine and Biology Society*, vol. 1, 2009, pp. 1016–1019.

[3] D. Knowles, D. Sudar, C. Bator-Kelly, M. Bissell, and S. Lelièvre, "Automated local bright feature image analysis of nuclear protein distribution identifies changes in tissue phenotype," *Proceedings of the National Academy of Sciences*, vol. 103, no. 12, pp. 4445–4450, 2006.

[4] N. Harder, F. Mora-Bermudez, and W. G. et al., "Automatic analysis of dividing cells in live cell movies to detect mitotic delays and correlate phenotypes in time," *Genome Research*, vol. 19, no. 11, pp. 2113–2124, 2009.

[5] E. Meijering, O. Dzyubachyk, I. Smal, and W. van Cappellen, "Tracking in cell and developmental biology," in *Seminars in Cell and Developmental Biology*. Elsevier, 2009, pp. 894–902.

[6] I. Ersoy, F. Bunyak, V. Chagin, M. Cardoso, and K. Palaniappan, "Segmentation and classification of cell cycle phases in fluorescence imaging," in *Medical Image Computing and Computer-Assisted Intervention (MICCAI)*, 2009, pp. 617–624.

[7] H. Leonhardt, H. Rahn, P. Weinzierl, A. Sporbert, T. Cremer, D. Zink, and M. Cardoso, "Dynamics of DNA replication factories in living cells," *Journal of Cell Biology*, vol. 149, no. 2, p. 271, 2000.

[8] A. Sporbert, A. Gahl, R. Ankerhold, H. Leonhardt, and M. Cardoso, "DNA polymerase clamp shows little turnover at established replication sites but sequential de novo assembly at adjacent origin clusters," *Molecular cell*, vol. 10, no. 6, pp. 1355–1365, 2002.

[9] D. Demandolx and J. Davoust, "Multicolour analysis and local image correlation in confocal microscopy," *Journal of Microscopy*, vol. 185, no. 1, pp. 21–36, 1997.

[10] A. Smallcombe, "Multicolor imaging: the important question of co-localization," *Biotechniques*, vol. 30, no. 6, pp. 1240–1247, 2001.

[11] F. Bunyak, K. Palaniappan, V. Chagin, and M. Cardoso, "Cell segmentation in time-lapse fluorescence microscopy with temporally varying sub-cellular fusion protein patterns," in *Int. Conf. of the IEEE Engineering in Medicine and Biology Society*, 2009, pp. 1424–1428.

[12] F. Bunyak, K. Palaniappan, S. K. Nath, T. Baskin, and G. Dong, "Quantitative cell motility for *in vitro* wound healing using level set-based active contour tracking," in *Proc. 3^{rd} IEEE Int. Symp. Biomed. Imaging (ISBI)*, April 2006, pp. 1040–1043.

[13] D. Padfield, J. Rittscher, T. Sebastian, N. Thomas, and B. Roysam, "Spatio-temporal cell cycle analysis using 3D level set segmentation of unstained nuclei in line scan confocal fluorescence images," in *3rd IEEE International Symposium on Biomedical Imaging: Nano to Macro, 2006*, 2006, pp. 1036–1039.

[14] A. Frangi, W. Niessen, K. Vincken, and M. Viergever, "Multiscale vessel enhancement filtering," in *Medical Image Computing and Computer-Assisted Intervention (MICCAI)*, 1998, pp. 130–137.

[15] R. Kerekes, S. Gleason, N. Trivedi, and D. Solecki, "Automated 3-D tracking of centrosomes in sequences of confocal image stacks," in *Int. Conf. of the IEEE Engineering in Medicine and Biology Society*, vol. 1, 2009, pp. 6994–6997.

[16] C. Westin, S. Maier, H. Mamata, A. Nabavi, F. Jolesz, and R. Kikinis, "Processing and visualization for diffusion tensor MRI," *Medical Image Analysis*, vol. 6, no. 2, pp. 93–108, 2002.